Acta Cryst. (1996). D**52**, 143–155

Structure Solution of a Cubic Crystal of Concanavalin A Complexed with Methyl α-D-Glucopyranoside

S. J. HARROP,[a] J. R HELLIWELL,[a]* T. C. M. WAN,[a]† A. J. KALB (GILBOA),[b]‡ LIANG TONG[c]§ AND J. YARIV[b]¶

[a]*Department of Chemistry, University of Manchester M13 9PL, England,* [b]*Department of Biophysics, Weizmann Institute, Rehovot, Israel, and* [c]*Department of Biological Sciences, Purdue University, West Lafayette, Indiana 47906, USA. E-mail: hell@man.ac.uk*

(Received 20 May 1995; accepted 28 June 1995)

Abstract

The solution of the cubic crystal form ($a = 167.8$ Å) of concanavalin A complexed with the monosaccharide methyl α-D-glucopyranoside is described. The space group has been determined as $I2_13$ rather than $I23$. The use of cadmium to replace cobalt at the transition metal-ion binding site and to replace calcium at its binding site proved to be crucial to the successful solution of the crystal structure. The relatively small isomorphous signals of 21 e^- for the replacement of cobalt and 28 e^- for the replacement of calcium, yielded interpretable difference Patterson maps. The electron-density map calculated in space group $I2_13$ at 5.4 Å resolution, based on phases derived from single- and double-substituted cadmium differences, revealed a classical concanavalin A tetramer of 222 point symmetry, as seen in all the known crystal structures of concanavalin A. Rigid-body refinement at 3.6 Å using the refined coordinates of saccharide-free concanavalin A converged to an R factor of 27.4%. A molecular-replacement analysis, consistent with this crystal structure, and initial experiences in the incorrect space group $I23$ are described as these also prove to be instructive.

1. Introduction

High-quality crystals of concanavalin A with bound saccharide have proved difficult to produce. In recent years the crystallographic analysis of concanavalin A complexed with methyl α-D-mannopyranoside (αMM) has been reported at 2.9 Å (Derewenda *et al.*, 1989) and subsequently at 2.0 Å resolution (Naismith *et al.*, 1994). The latter paper also gave the comparison of the αMM concanavalin A complex structure at 2.0 Å resolution with the saccharide-free concanavalin A structure at 1.6 Å resolution.

The crystallization of concanavalin A complexed with methyl α-D-glucopyranoside (αMG) was reported some years ago (Yariv *et al.*, 1987), before the αMM concanavalin A complex, and yet the crystal structure solution of this cubic form has proved difficult. The crystal structure has now been solved and is reported here. Although the structure of concanavalin A is well known, it was necessary to use multiple isomorphous replacement to directly calculate phases and electron-density maps for this crystal form. Initial molecular-replacement calculations in this high-symmetry crystal proved impossible to interpret, owing to the preponderance of symmetry related peaks in the rotation and translation maps (see *Appendix A*). Finally, the interpretation in space group $I2_13$ yielded a very clear electron-density map, with the tetrameric quaternary arrangement, familiar in concanavalin A structural studies, being clearly discernible. Our initial crystallographic investigations utilizing a K_2PtCl_4 heavy-atom derivative seemed to indicate that an interpretation of the resulting isomorphous difference Patterson in space group $I23$ was correct rather than $I2_13$. This also seemed to be consistent with iron-uptake experiments in aqueous solution, as well as the high solvent content of these crystals, suggesting that concanavalin A might resemble ferritin, which is composed of 24 identical monomers arranged as a closed shell of 432 point symmetry (Yariv *et al.*, 1988). Such a shell, comprised of 12 dimers of concanavalin A, would be compatible with space group $I23$ if placed around the body centre of the unit cell. Finally, we can now describe the correct crystal structure in space group $I2_13$ as determined by isomorphous replacement. The derivatization involved replacing the transition metal or the calcium ion with cadmium, in two different combinations [Kalb (Gilboa), Yariv, Helliwell & Papiz, 1988]. Such a substitution (Weinzierl & Kalb, 1971) results in fairly small isomorphous differences. However, this did not prove to be a handicap. Firstly, we used an electronic area detector. Secondly, the crystal properties were favourable, namely their cubic symmetry, their excellent quality and their stability in the beam. Hence, these factors allowed us to obtain a high data redundancy (up to 30-fold at 5.4 Å resolution) and accurate measure-

† Current Address: Department of Biophysics, King's College, University of London, England.
‡ Current Address: Department of Structural Biology, Weizmann Institute, Rehovot, Israel.
§ Current Address: Boehringer Ingelheim Pharmaceuticals Inc., 900 Ridgebury Road, PO Box 368, Ridgefield, CT 06877, USA.
¶ Current Address: Université Bordeaux 1, Talence, Bordeaux, France.

ments of the small intensity differences resulting from the substitution.

The ultimate interest in solving this crystal structure complex lies in the further knowledge and detailed understanding that can be gained of concanavalin A monosaccharide interactions. In particular the detailed comparison of the αMG and αMM binding modes is of structural and thermodynamic interest; a brief report of such a comparison has been presented at the Beijing Congress (Harrop *et al.*, 1993) and will be reported in detail elsewhere.

2. Materials and methods

2.1. *Crystallization, unit cell and space group*

Full details and an estimate of the protein content were given in Yariv *et al.* (1987) and so only a brief summary is given here. Crystals of the αMG concanavalin A complex were grown by dialysis at a protein concentration of approximately 5 m*M* with 0.1 *M* αMG and 1.8 *M* sodium phosphate at pH 6.8. The crystals grow as regular rhombic dodecahedra and reach a size of 1 mm^3 in a few days (Fig. 1). In some cases they attain a maximum dimension of 5 mm! The crystals are handled in a synthetic mother liquor of composition 1.8 *M* sodium phosphate, 5 mg ml^{-1} concanavalin A and 0.1 *M* αMG. The space group and unit-cell parameters were determined using precession photography. The symmetry and systematic absences are consistent with the cubic space group $I23$ or $I2_13$ with unit-cell edge, $a = 167.8$ Å. The molecular weight of the protein in the asymmetric unit was determined by direct measurement of crystal density and protein content to be 50.3 kDa corresponding to a dimer of concanavalin A. The crystal volume per unit of protein mass, V_m is very high: 3.91 $Å^3$ Da^{-1} compared to 2.35 $Å^3$ Da^{-1} for the orthorhombic saccharide-free form.

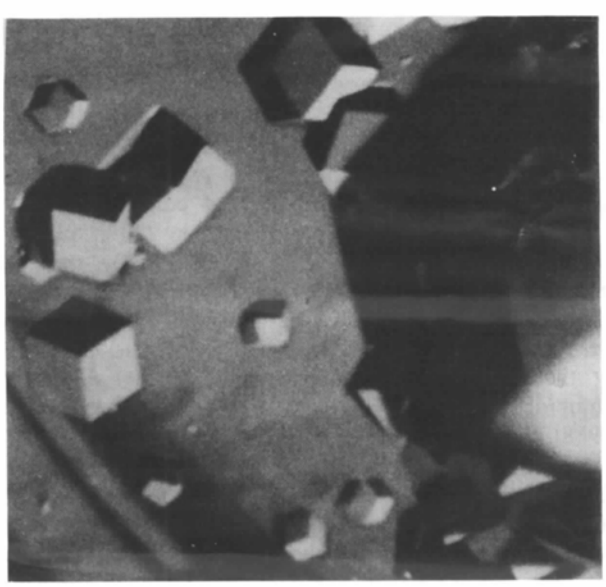

Fig. 1. Photograph of typical crystals of concanavalin A and αMG. The crystals grow as regular rhombic dodecahedra reaching 1 × 1 × 1 mm within a few days. Larger crystals can be grown.

2.2. *X-ray data collection*

High-quality X-ray diffraction data were collected on a Xentronics MWPC installed and calibrated on a sealed tube Cu $K\alpha$ X-ray source (Derewenda & Helliwell, 1989). Native data were collected to 3.6 Å. 'Native' means that, as prepared, these crystals of concanavalin A have a mixed population of transition metals in the transition metal binding site (*S*1). Derivative data sets were then collected at approximately 5 Å resolution from crystals in which the transition metal in the site *S*1 was selectively replaced with Cd^{2+} or Co^{2+}. The Ca^{2+} ion in the adjacent calcium ion binding site [4.16 Å away (Naismith *et al.*, 1993)] can also be replaced with Cd^{2+} owing to their similar ionic radii (Shoham, Kalb & Pecht, 1973). This site is referred to as *S*2. Hence, very closely isomorphous crystals can be prepared with different combinations of metals in the *S*1 and *S*2 sites [see Kalb (Gilboa) *et al.*, 1988 for a discussion with respect to the saccharide-free crystal form]. The crystal data sets are then identified by the labelling convention [*S*1:*S*2]; for example, a data set labelled [Cd:Ca] represents data collected from concanavalin A that has been prepared so that *S*1 contains only Cd and *S*2 only Ca. Three sets of crystals prepared in this way are of special relevance to the solution of this crystal structure, namely [Cd:Cd], [Cd:Ca] and [Co:Ca]. A data set was also collected on a K_2PtCl_4 heavy-atom derivative of native (mixed metal) cubic crystals, as this had been identified as a suitable derivative to bind to concanavalin A from the saccharide-free $I222$ crystal structure solution (Greer, Kaufman & Kalb, 1970; Reeke, Becker & Quiocho, 1971; Hardman & Ainsworth, 1972) and its metal-free $P2_122_1$ crystal form (Shoham *et al.*, 1979).

The geometry of the derivative data collection at 5.4 Å involved a symmetric setting of the MWPC (tilt angle 0°) and a detector distance from the crystal of 170 mm set so as to resolve the diffraction spots on the detector surface. However, in two cases a tilt angle of 6° and a crystal-to-detector distance of 230 mm was required to resolve adjacent spots. Data were generally collected with a high redundancy. Individual frames of 0.25° were exposed. In the case of the 3.6 Å data the detector was tilted by 12°. A summary of the experimental details is given in Table 1. The [Co:Ca] data set was collected with a strategy to enhance the accuracy of the f'' anomalous signal of Co (*K* edge 1.608 Å) with the Cu $K\alpha$ wavelength of 1.5418 Å. (Unfortunately, the anomalous difference Patterson map for the cobalt data was relatively featureless.) Data were indexed and processed with the *Xengen* software (Howard *et al.*, 1987). The high data redundancy and overall completeness

Table 1. *Details of the Xentronics MWPC area detector data collection at Cu Kα wavelength*

Data set	Exposure time per 0.25° frame (s)	Crystal-to-detector distance (mm)	Tilt angle (°)	Degrees of data collected (°)	Resolution of data (Å)	$N_{observed}$	N_{unique}	Overall completeness (%)	R_{merge} (*I*)* (%)	$\Delta F/F$ (%)†
Native	350	230	12	107	3.6	25777	8740	94	6.1	5.0
K_2PtCl_4	500	230	6	107	5.0	19467	3635	99	7.8	20.5
[Co:Ca]	350	170	0	280	5.4	67241	2936	98	6.7	—
[Cd:Ca]	350	230	6	223	5.0	74029	3939	99	10.1	6.6
[Cd:Cd]	200	170	0	160	5.3	47672	3091	98	8.8	9.4

* $R_{merge} = \sum |I - \langle I \rangle| \sum I$. † $\Delta F/F = \left(\sum |F1 - F2| / \sum F1 \right) \times 100$. Where $F1$ and $F2$ are the structure-factor amplitudes from data sets 1 and 2, respectively, and calculated against the [Co:Ca] data. In order to calculate isomorphous differences a feature of this space group is that data sets from separate crystals must be brought to a common orientation. This is readily done by exchanging the h and k indices as necessary. The significance of this can be visualized *via* a precession photograph or plot of the $hk0$ zone intensities.

should be noted for the derivative data sets, especially the *S*1 and *S*2 substituted forms (Table 1). Moreover, the different $\Delta F/F$ values indicate the error and signal levels. An indication of the error level is given by the native to [Co:Ca] data sets with a $\Delta F/F$ of 5.0%. There is an increase in $\Delta F/F$ signal as we progress from the [Cd:Ca] *versus* [Co:Ca], of 6.6% and then to [Cd:Cd] *versus* [Co:Ca] of 9.4%. The largest difference is for the K_2PtCl_4 derivative with a $\Delta F/F$ of 20.5%. These data sets were used to calculate various isomorphous difference Patterson maps; the case of the K_2PtCl_4 is dealt with in *Appendix B* as it led to erroneous results as it turned out.

2.3. *Interpretation of isomorphous difference Patterson maps*

The correct choice of space group between *I*23 and $I2_13$, and the location of each pair of [*S*1:*S*2] sites in the dimer in the crystallographic asymmetric unit, was achieved *via* the isomorphous difference Patterson maps. Table 2 summarizes the symmetry properties of space groups *I*23 and $I2_13$ as well as those of the corresponding Patterson space. From Table 2(*c*) it can be seen that *I*23 and $I2_13$ have the same Patterson-symmetry space group ($Im\bar{3}$) and the same Harker sections. However, they have different Harker vectors. Hence, a distinction can be made between the two space groups, by interpreting the isomorphous difference Patterson maps. Such a choice was previously not possible from systematic absences in the diffraction pattern alone.

Difference Patterson maps were calculated from various pairs of data sets. Conventionally one set is regarded as a 'native' set against which the derivative data sets are compared. However, in this study it proved absolutely essential to vary also the set treated as the native set. Hence, a variety of pair-wise combinations were taken. In this way, by taking combinations of pairs from the three sets [Co:Ca], [Cd:Ca] and [Cd:Cd] it was possible to calculate isomorphous difference Patterson maps that contained vectors arising from only a single species of site (*i.e.* *S*1 or *S*2) as well as from both sites. Two

Table 2. *Details of the crystal (I23/I2$_1$3) and Patterson ($Im\bar{3}$) space groups*

(*a*) Equivalent positions

*I*23 (0,0,0); $(\frac{1}{2},\frac{1}{2},\frac{1}{2})$			$I2_13$ (0,0,0); $(\frac{1}{2},\frac{1}{2},\frac{1}{2})$		
xyz	yzx	zxy	xyz	yzx	zxy
$x\bar{y}\bar{z}$	$y\bar{z}\bar{x}$	$z\bar{x}\bar{y}$	$\frac{1}{2}+x, \frac{1}{2}-y, \bar{z}$	$\frac{1}{2}+y, \frac{1}{2}-z, \bar{x}$	$\frac{1}{2}+z, \frac{1}{2}-x, \bar{y}$
$\bar{x}\bar{y}z$	$\bar{y}\bar{z}x$	$\bar{z}\bar{x}y$	$\frac{1}{2}-x, \bar{y}, \frac{1}{2}+z$	$\frac{1}{2}-y, \bar{z}, \frac{1}{2}+x$	$\frac{1}{2}-z, \bar{x}, \frac{1}{2}+y$
$\bar{x}yz$	$\bar{y}zx$	$\bar{z}xy$	$\bar{x}, \frac{1}{2}+y, \frac{1}{2}-z$	$\bar{y}, \frac{1}{2}+z, \frac{1}{2}-x$	$\bar{z}, \frac{1}{2}+x, \frac{1}{2}-y$

(*b*) Equivalent positions in the Patterson space group $Im\bar{3}$, (0,0,0), $(\frac{1}{2},\frac{1}{2},\frac{1}{2})$.

xyz	yzx	zxy	$\bar{x}\bar{y}\bar{z}$	$\bar{y}\bar{z}\bar{x}$	$\bar{z}\bar{x}\bar{y}$
$x\bar{y}\bar{z}$	$y\bar{z}\bar{x}$	$z\bar{x}\bar{y}$	$\bar{x}yz$	$\bar{y}zx$	$\bar{z}xy$
$\bar{x}\bar{y}z$	$\bar{y}\bar{z}x$	$\bar{z}\bar{x}y$	$xy\bar{z}$	$yz\bar{x}$	$z\bar{x}\bar{y}$
$\bar{x}y\bar{z}$	$\bar{y}z\bar{x}$	$\bar{z}x\bar{y}$	$x\bar{y}z$	$y\bar{z}x$	$z\bar{x}y$

(*c*) Harker vectors in the Patterson space group $Im\bar{3}$ for

*I*23	$I2_13$
$2x, 2y, 0$	$2x, 2y+\frac{1}{2}, 0$
$2y, 2z, 0$	$2y, 2z+\frac{1}{2}, 0$
$2z, 2x, 0$	$2z, 2x+\frac{1}{2}, 0$
etc.	

Table 3. *Mean fractional isomorphous differences ($\Delta F/F$) between data sets (%)*

Upper triangle, experimental values; lower triangle, theoretical values (based on the final solution).

	[Co:Ca]	[Cd:Ca]	[Cd:Cd]
[Co:Ca]	—	6.6	9.4
[Cd:Ca]	5.3	—	7.2
[Cd:Cd]	7.9	7.0	—

difference Patterson maps were essential for the solution of this crystal structure. First the Patterson derived from the coefficient ([Cd:Ca]–[Co:Ca]) has an intrinsic signal of 21 e^- from each of the two *S*1 sites in the asymmetric unit. Secondly, the Patterson map derived from the coefficient ([Cd:Cd]–[Cd:Ca]) has an intrinsic signal of 28 e^- from each of the two *S*2 sites. Table 3 gives the $\langle \Delta F/F \rangle$ values for each pair wise combination of data sets. With two subunits of concanavalin A per crystallographic subunit (referred to as *A* and *B*), two *S*1 and two *S*2 sites per asymmetric unit are expected. There are 24 asymmetric units per unit cell in *I*23 or $I2_13$. Clearly, a Harker section containing peaks from the 2*S*1

or 2S2 sites alone should be much easier to interpret than one containing all four sites (*i.e.* 2S1 + 2S2).

The Harker sections from the [Cd:Ca]–[Co:Ca] and [Cd:Cd]–[Cd:Ca] calculations are shown in Figs. 2(*a*) and 2(*b*). The interpretation of these Patterson maps is simplified if they are studied in parallel as a pair, although Fig. 2(*b*) is of outstanding clarity and was the map yielding the breakthrough for the solution of this crystal structure. Each site in the real-space cell will yield a triplet of peaks on the $W = 0$ Harker section; the $U = 0$ and $V = 0$ Harker sections are identical to the one at $W = 0$. As the S1–S2 distance in a concanavalin A monomer is 4.16 Å, we expect to find a given set of Harker triplets slightly displaced from another set by 2×4.16 Å in the two Patterson maps.

In each map a set of three peaks on the $W = 0$ Harker can be seen arising from subunits *A* and *B* in the asymmetric unit of an $I2_13$ unit cell. The vectors arising from the *A* subunit are particularly clear (marked VAA) on Fig. 2. No satisfactory interpretation could be made in space group *I*23.

As the asymmetric unit contains a dimer a second set of vectors for subunit *B* in each map is expected. The Harker triplets of peaks belonging to these sites in the second monomer are marked •VBB. The positions of these sites were not recovered from inspection of the Patterson in fact but from difference Fourier maps (see §2.4). Whilst significant peaks are present for all the calculated positions the interpretation of the *B* subunit sites is not as clear as that for the *A* subunit set described above. Moreover by having two subunits (each with S1 + S2 sites) per asymmetric unit there are crossvectors between sites. For this crystal structure the interpretation of the Patterson maps is complicated because many of the vectors lie close to or on the Harker $W = 0$ plane and so increase the complexity of the interpretation. This was especially troublesome in the K_2PtCl_4 Patterson map discussed in *Appendix B*.

On the basis of a partial solution, in $I2_13$, involving the location of one pair of metal binding sites (*i.e.* S1 and S2 in subunit *A*), and with no satisfactory solution in *I*23, the analysis of the isomorphous data was continued in space group $I2_13$.

2.4. *Interpretation of isomorphous difference Fourier maps*

Only the S1 and S2 sites for the *A* subunit in the asymmetric unit were explicitly derived from the Patterson maps in §2.3. The remaining metal sites for subunit *B* were located from difference Fourier maps, with phases calculated from a partial model of the independent sites. Subsequently the corresponding peaks in the relevant Patterson maps were identified, as mentioned in §2.3 above.

2.4.1. *S1 sites.* A Fourier map with coefficients {[Cd:Ca]–[Co:Ca]} with single isomorphous replacement (SIR) phases calculated from a single S2 site (subunit *A*) located from the {[Cd:Cd]–[Cd:Ca]} Patterson map clearly shows two S1 sites per asymmetric unit. Fig. 3 shows sections of this map. One S1 site

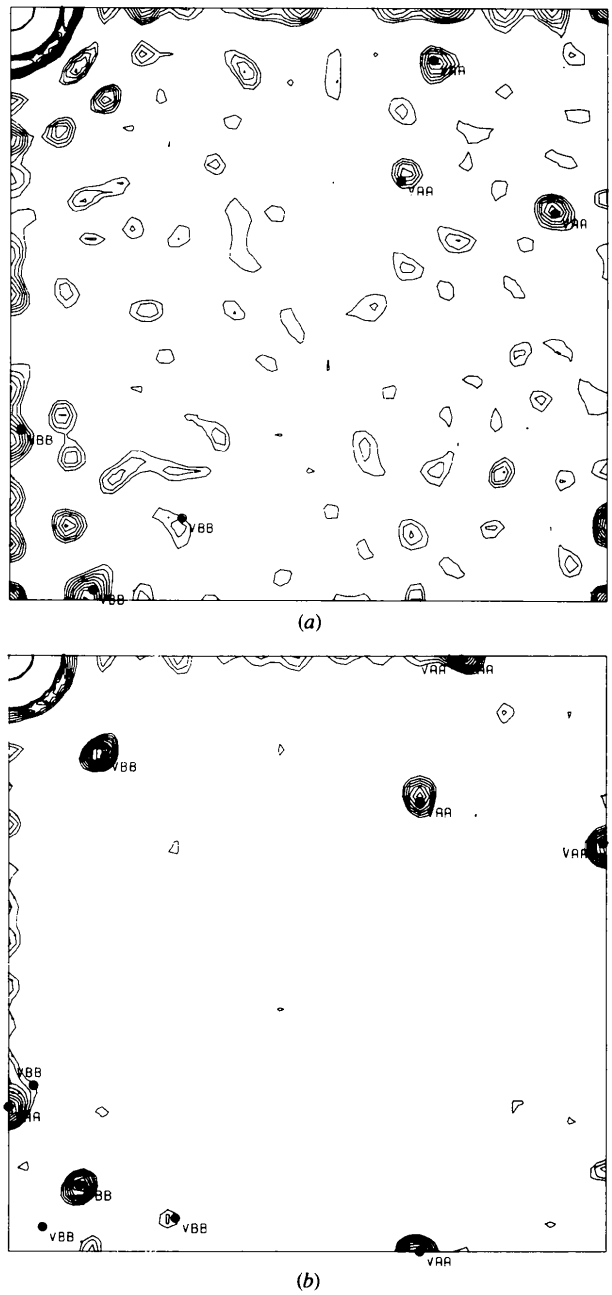

Fig. 2. Isomorphous difference Patterson maps. (*a*) {[Cd:Ca]–[Co:Ca]}. A 21 e^- signal from the S1 sites in subunits *A* and *B*. (*b*) {[Cd:Cd]–[Cd:Ca]}. A 28 e^- signal from the S2 sites in subunits *A* and *B*. The triplet of Harker vectors from the sites identified from the Patterson maps are marked AA. Those marked BB are from vectors for the sites for subunit *B* located from difference Fourier maps. The $W = 0$ Harker sections are shown with the origin at top left with *x* running vertical and *y* horizontal, both from 0 to 1/2.

(subunit *A*) is the same as that recovered from the interpretation of the {[Cd:Ca]–[Co:Ca]} Patterson map. The second *S*1 site (subunit *B*) is the remaining site as expected for a dimer in the asymmetric unit. No other significant peaks were found in the difference Fourier map. The positions of the two *S*1 sites were refined as detailed in §2.5 and Table 4(*a*).

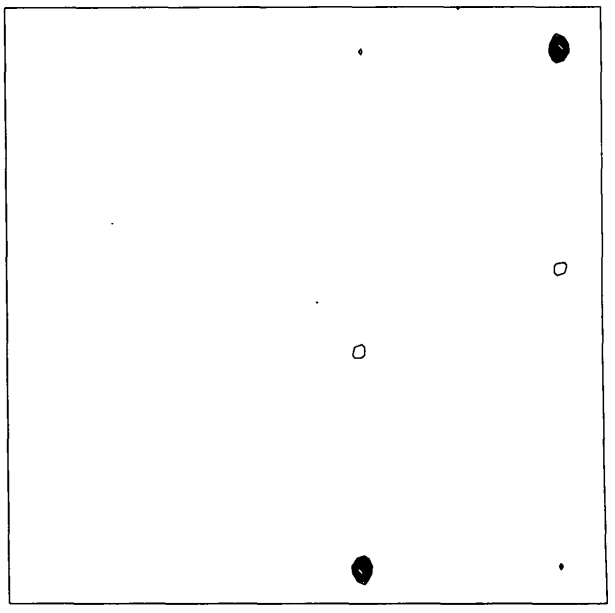

(*a*)

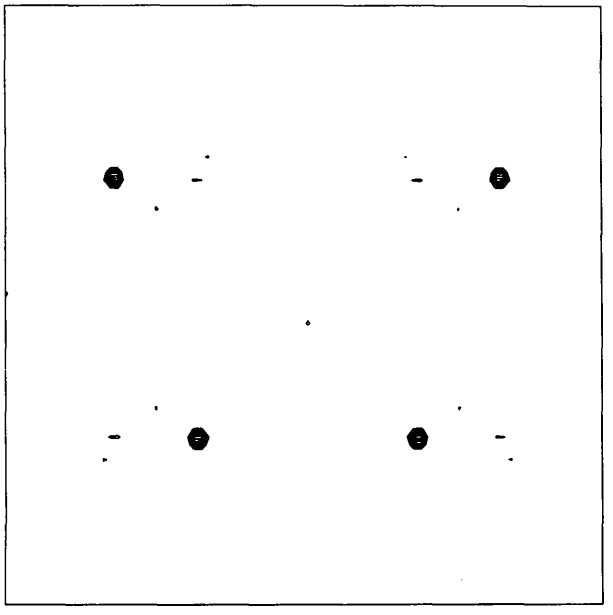

(*b*)

Fig. 3. {[Cd:Ca]–[Co:Ca]} difference Fourier map with SIR phases based on the *S*2 site of subunit *A* and which shows the *S*1 sites per asymmetric unit *i.e.* subunit *A* and *B*. (*a*) Section $y = 2/80$, (*b*) section $y = 20/80$. Maps contoured from 3σ in intervals of 1σ. The whole unit cell in x and z is shown.

Table 4. *SCFHLE refinement of S1 and S2 sites*

(*a*) *S*1 sites [Cd:Ca] *versus* [Co:Ca] in subunits *A* and *B* at 5.4 Å

Site	Occupancy	Fractional coordinates x	y	z	*B* factor (Å^2)*
*S*1.*A*	0.45	0.0730	0.0867	0.4781	15
*S*1.*B*	0.42	0.2849	0.1800	0.2455	15

(*b*) *S*2 sites [Cd:Cd] *versus* [Cd:Ca] in subunits *A* and *B* at 5.4 Å

Site	Occupancy	Fractional coordinates x	y	z	*B* factor (Å^2)*
*S*2.*A*	0.56	0.0608	0.0781	0.4986	15
*S*2.*B*	0.48	0.2642	0.1804	0.2606	15

(*c*) Refinement statistics

	*S*1.*A* + *S*1.*B*	*S*2.*A* + *S*2.*B*
No. of reflections in refinement	253	247
R_{Cullis}†	0.35	0.35
Gradient‡	0.71	0.59
Correlation§	0.77	0.75
Phasing power F_H/E¶	2.42	2.34

* *B* factor is the isotropic temperature factor defined by the expression $\{\exp[-B(\sin\theta/\lambda)^2]\}$. † $R_{Cullis} = \sum ||F_{PH} \pm F_P| - F_H(\text{calc})| / \sum |F_{PH} - F_P|$, where F_P and F_{PH} are the structure-factor amplitudes of the protein and heavy-atom derivative, respectively, and F_H(calc) is the calculated heavy-atom structure-factor amplitude summed over centric data only. ‡ Gradient is the gradient of the least-squares straight line with F_{obs} as the ordinate and F_{calc} as the abscissa. § Correlation is the correlation coefficient between F_{obs} and F_{calc} defined as $C = [\sum_h (\langle F_{obs}\rangle - |F_{obs}|)(\langle F_{calc}\rangle - |F_{calc}|)] / [\sum_h (\langle F_{obs}\rangle - |F_{obs}|)^2 (\langle F_{calc}\rangle - |F_{calc}|)^2]^{1/2}$. ¶ Phasing power $= F_H/E$, the r.m.s. heavy-atom structure-factor amplitudes divided by the residual lack-of-closure error.

2.4.2. *Confirmation of S2 sites from S1 sites.* The *S*2 sites could be located from a difference Fourier map with coefficients {[Cd:Cd]–[Cd:Ca]} phased using SIR phases calculated from the two-site model of *S*1 sites found above (§2.4.1). This clearly showed two *S*2 sites per asymmetric unit. The sites are expected 4.16 Å distant from the *S*1 sites located in the previous map. Again one site corresponds to the site recovered from the {[Cd:Cd]–[Cd:Ca]} Patterson map (subunit *A*), the other to the expected second site (subunit *B*). No other significant peaks were located in the map. The positions of these two sites were then refined (§2.5 and Table 4*b*).

2.4.3. *Pt sites.* Double isomorphous replacement (DIR) phases caculated from the [Cd:Cd] and [Cd:Ca] *versus* [Co:Ca] data were used to phase a {Pt[Native:Ca]–[Co:Ca]} difference Fourier map. Four Pt sites were located, two major and two minor sites per asymmetric unit. This is consistent with the known binding behaviour of K_2PtCl_4 to concanavalin A in its saccharide-free *I*222 crystal form (Greer *et al.*, 1970; Reeke *et al.*, 1971; Hardman & Ainsworth, 1972) and in its metal-free $P2_122_1$ crystal form, Shoham *et al.*, 1979), where the major Pt sites involved Met129 and the minor Pt sites, Met42. The positions of the four sites were then refined. As a cross check SIR phases were calculated form this four-site Pt model and used to phase a {[Cd:Cd]–[Co:Ca]} difference map. The *S*1 and *S*2 sites in subunits *A* and *B* were easily located

and no new sites were identified from the map. The predicted positions of the vectors on the $W=0$ Harker section for the Pt derivative in the space group $I2_13$ explained nearly all the major peaks on the Patterson map (see Fig. 10).

2.5. *Refinement of the metal sites*

The occupancies and positions of the metal-ion and Pt sites were refined against centric data only using the *SCFHLE* [centric heavy-atom lower estimate (Dodson & Vijayan, 1971)] option in the *CCP*4 (Collaborative Computational Project, Number 4, 1994) program *REFINE*. Data between 15 and 5.4 Å were used. The final parameters used for the calculation of protein phases together with some statistics on the quality of the refinement are given in Tables 4–6. *B* factors were set to 15 Å^2 and were not refined because at this low resolution *B* values are highly correlated to occupancies.

The parameters for the *S*1 and *S*2 sites were refined using the 21$^-$ and 28 e$^-$ per site isomorphous-difference signals. The *S*1 sites were refined against [Cd:Ca] *versus* [Co:Ca] data and the *S*2 sites were refined against the [Cd:Cd] *versus* [Cd:Ca] data. The form factor for the difference signals was modelled using the parameters for Cd (nominally set at 48 e$^-$). Hence, the occupancy was allowed to refine to an appropriate value to account for the difference between 48 e$^-$ and the actual signals of 21 e$^-$ and 28 e$^-$. The *S*1 and *S*2 sites were then refined simultaneously using [Cd:Cd] *versus* [Co:Ca] data. The parameters for the four Pt sites were refined using K_2PtCl_4 *versus* [Co:Ca] data. The difference between the mixed metal *S*1 site in the K_2PtCl_4 derivative of the native crystal, and the homogeneous *S*1 site in [Co:Ca], is around 2 e$^-$ and is, therefore, negligible. No problems were encountered during the refinement and all parameters converged smoothly. Indeed, the high degree of isomorphism between the metal-ion exchange crystals, and the high quality of the data, is reflected in the exceptional quality of the isomorphous-refinement statistics.

2.6. *Phasing and the electron-density map at 5.4 Å*

Isomorphous-replacement phases were calculated at 5.4 Å using the *CCP*4 (Collaborative Computational Project, Number 4, 1994) program *PHASE*2 which uses the Blow & Crick (1959) statistical error model of isomorphous replacement to calculate protein phase angles and define a phase-probability distribution. The [Co:Ca] data were now considered as the 'native' and the [Cd:Cd], [Cd:Ca] and K_2PtCl_4 data considered as 'derivatives'. Two phase sets were calculated; an MIR phase set using all three derivative data sets, and a set of DIR phases using only the isomorphous signals from the [Cd:Cd] and [Cd:Ca] data. This DIR phase set was used to judge if the project could have been completed from the metal-ion exchange data sets alone.

Table 5. *SCFHLE refinement of the S1 and S2 sites simultaneously, [Cd:Cd] versus TR:[Co:Ca]*

For definition of symbols see Table 4.

Site	Occupancy	*x*	*y*	*z*	*B* factor (Å^2)
*S*1.*A*	0.38	0.0712	0.0881	0.4771	15
*S*1.*B*	0.41	0.2870	0.1800	0.2440	15
*S*2.*A*	0.61	0.0608	0.0785	0.4972	15
*S*2.*B*	0.52	0.2644	0.1807	0.2587	15

No. of reflections in refinement	252
R_{Cullis}	0.34
Gradient	0.66
Correlation	0.78
F_H/E	2.43

Table 6. *Centric SCFHLE refinement of the Pt positions, K_2PtCl_4 derivative versus [Co:Ca] data at 5.4 Å*

For definitions of symbols see Table 4.

Site	Occupancy	*x*	*y*	*z*	*B* factor (Å^2)
1.*A*	0.77	0.4127	−0.0072	0.2308	15
1.*B*	0.88	0.3491	0.0130	0.2630	15
2.*A*	0.27	0.6342	0.0440	0.5634	15
2.*B*	0.32	0.2212	0.1356	0.2328	15

No. of reflections in refinement	240
R_{Cullis}	0.39
Gradient	0.57
Correlation	0.70
F_H/E	2.07

This is a fair calculation as the positions of the *S*1 and *S*2 sites were located and refined without reference to the K_2PtCl_4 data.

Fig. 4 shows the figure of merit for the resulting phases for both the MIR and DIR phase sets. Overall for the MIR data set, 2749 reflections to 5.4 Å (92% complete) were phased with a mean figure of merit, $\langle m\rangle = 0.71$. This implies an average phase error of around 43°. For the DIR data set 2746 reflections to 5.4 Å (92% complete) were phased with $\langle m\rangle = 0.68$, an average phase error of around 47°. These two phase sets were used to calculate electron-density maps with coefficients,

$$mF_{|Co:Ca|}\exp(i\alpha),$$

where m is the figure of merit for each reflection and α is the calculated centroid best phase. Fig. 5(*a*) shows a representative 13 Å thick slab of the resulting electron-density map for the MIR phases, and Fig. 5(*b*) the same slab for the DIR phases. The electron-density maps have not been subjected to any solvent flattening or phase-improvement procedure. Both maps show a clear solvent protein boundary. Inspection of either of the maps shows that the asymmetric unit consists of a dimer in a general position with the quaternary structure of concanavalin A in the crystal being the standard concanavalin A tetramer observed in all other concanavalin A crystal structures studied to date (Fig. 5).

The DIR map is almost as interpretable as the MIR map. The figure-of-merit statistics (Fig. 4) show that the DIR phases calculated using the small isomorphous signals from the metal-ion exchange data sets are nearly as good as those from including the K_2PtCl_4 data.

2.7. *Placing concanavalin A subunits into the $I2_13$ unit cell*

A starting model could now be constructed by least-squares fitting of the *S*1 and *S*2 sites (four in all) onto the *S*1 and *S*2 sites within the unit cell using the refined model of the concanavalin A dimer (Naismith *et al.*, 1993). The positions of the *S*1 and *S*2 sites were plotted onto the 5.4 Å MIR minimap. The density was followed through the map whereby each monomer of the dimer could be identified. The *RIGI* option in *FRODO* for rigid-body least-squares minimization (Jones, 1978, as modified and distributed by P. Evans) was used to place the dimer onto the chosen guide atoms and to perform a distance minimization. To confirm the hand of the metal sites in the unit cell the minimization was performed on the site coordinates and then on their mirror image, which yielded r.m.s. differences of 0.1 and 3.2 Å, respectively. The original (arbitrary)

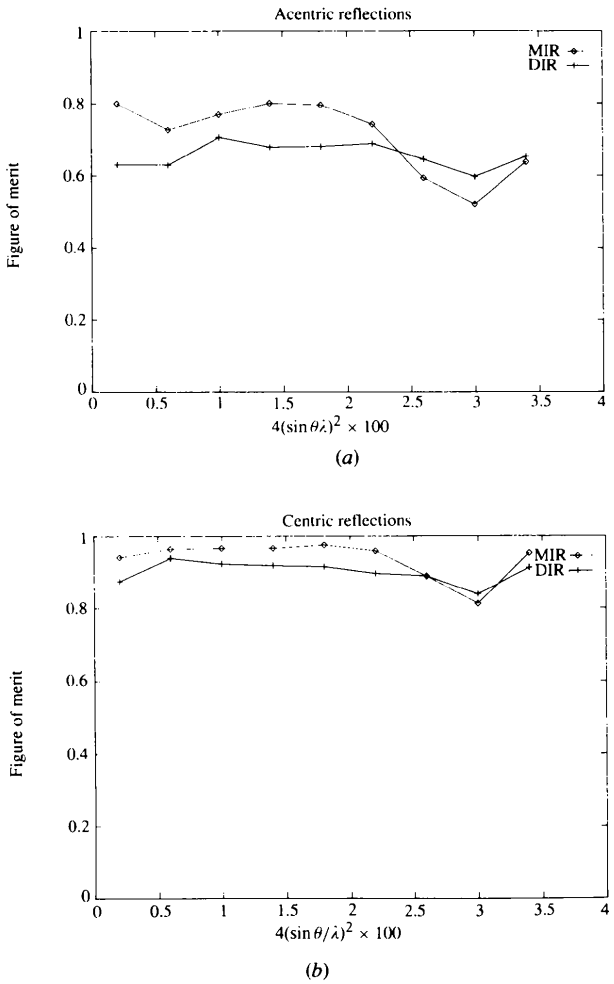

Fig. 4. Figures of merit of the MIR and DIR experimental phases plotted against resolution. (*a*) Acentrics, (*b*) centrics.

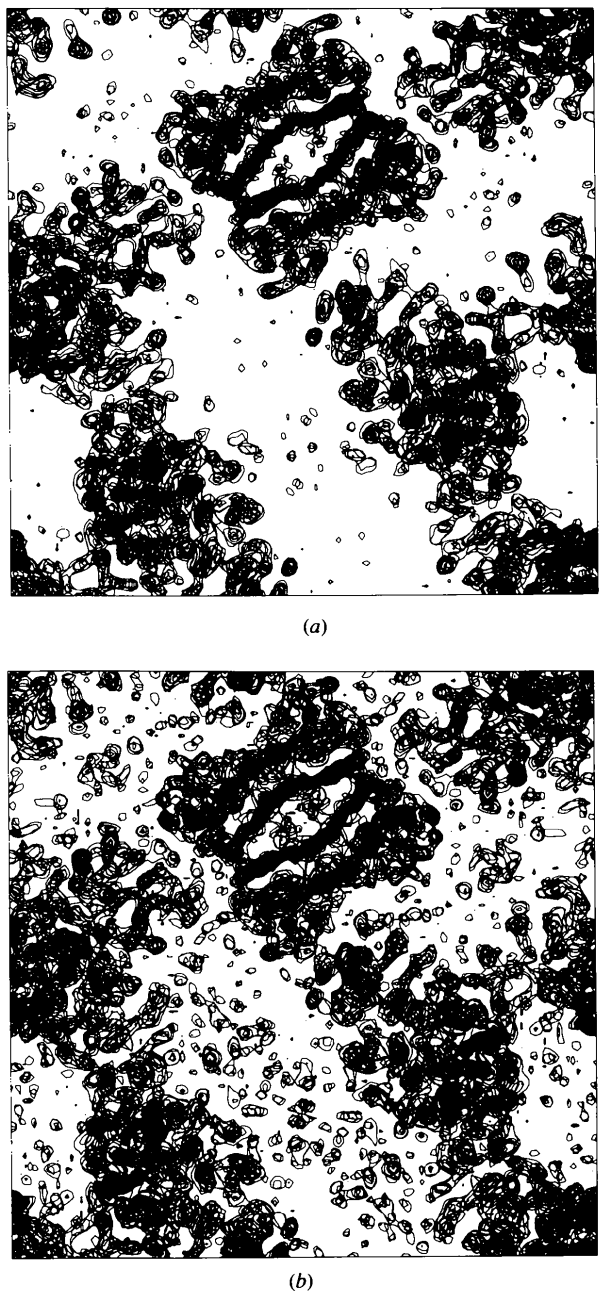

Fig. 5. Sections of the 5.4 Å electron-density map comprising a 13 Å thick slab through the unit cell contoured from 1 r.m.s. in 1 r.m.s. intervals. (*a*) MIR phases (*b*) DIR phases (*i.e.* excluding the Pt data). The whole unit cell in *x* and *y* is shown. In the minimaps clear electron density can be seen for a classical tetramer of concanavalin A.

choice of hand for the metal-ion structure was, therefore, confirmed as correct. At this stage the *R* factor for the complete model was 37.3% against the 5.4 Å [Co:Ca] data and 41.5% against the 3.6 Å native data for the correct hand.

The refinement of the concanavalin A dimer as a rigid body was then made using calculated structure amplitudes refined against the 3.6 Å native data by the method of Derewenda (1989), which has a large radius of convergence. The model was subjected to five cycles of least-squares positional refinement using the *TNT* suite (Tronrud, Ten Eyck & Matthews, 1987) followed by three cycles of *B*-factor refinement. For each monomer in the dimer, atoms within 12 Å of the molecular centre and having a *B* factor of less than 20 $Å^2$ were selected as a reference set. A concanavalin A monomer from the original model was then least-squares fitted to this reference set using the program *LSQKAB* (Kabsch, 1976). After each cycle of this procedure the resulting model is identical to the starting model save for a rigid-body movement of each of the monomers. The procedure was repeated four times. The *R* factor fell from a starting value of 41.5% to a final value of 27.4% at 3.6 Å. This then served as the start of a detailed model refinement, which will be described elsewhere, along with the details of the concanavalin A and αMG interactions.

3. Discussion and conclusions

This crystal structure was solved *via* specific metal-ion exchanges, based on the known behaviour of the concanavalin A molecule. The collection of X-ray data from each metal-ion exchanged type of crystal involved use of a very high crystallographic data redundancy so as to measure the ensuing small isomorphous intensity differences as exactly as possible. These metal-ion differences could then be refined with outstandingly good refinement statistics. The work was carried out at a resolution of 5 Å because the objective was to locate the known concanavalin A dimer structure in the asymmetric unit of this unit cell and then proceed *via* model refinement against higher resolution data. The 5 Å electron-density maps, without recourse to any solvent flattening, are of outstanding quality. We might expect a 3 Å map derived from similar data from a protein of unknown structure to be of such quality as to lead to interpretation of the structure provided the data are of high quality, and high redundancy to the resolution limit required. The situation of using small isomorphous differences in these metal-ion exchange data sets is analogous to synchrotron MAD data collection where small signals are extracted from highly redundant data sets. We would expect electron-density maps of exceptional quality to be produced providing that strict isomorphism would persist for the full resolution range.

The use of a classical heavy-atom derivative, the K_2PtCl_4 derivative, in this study proved to be unhelpful for several reasons. The special positions of the metal atoms in the unit cell, as determined from the metal-ion exchange phases, corresponded to a set of Harker peaks of which two were very close to the origin peak of the Patterson (Fig. 10). Also, it was most unfortunate that a noise peak on the K_2PtCl_4 $W=0$ Harker led to an interpretation of a triplet of peaks (Fig. 6) in what turned out to be the incorrect space group (*I*23). The single Pt derivative phases in *I*23 led to an electron-density map which, although it was of poor quality (Fig. 7), responded to solvent flattening in a way that led to a spherical shell of electron density around the body centre position (Fig. 8*b*) akin to that expected from earlier Mossbauer and iron-uptake experiments (Yariv *et al.*, 1988). However, this map (Fig. 8) was not continuous enough to allow interpretation in any sensible way, nor did it allow the placement of a concanavalin A molecule into it (see *Appendix B*). At this point of the project the emphasis shifted to a complete re-evaluation of the derivative and metal-ion exchange data sets. A critical step was to vary the data set used as the native so as to produce Patterson maps derived in turn from separate *S*1 and *S*2 sites (particularly Fig. 2*b*). In a high-symmetry space group this also controlled the number of peaks occurring in the Patterson map. It is also unfortunate that the molecular-replacement calculations proved impossible to interpret initially, for reasons discussed in *Appendix A*. In hindsight it seems that a large number of steps had to be taken to solve this crystal structure but the sequence still remains perfectly logical in terms of what was likely to allow a solution. A key point was that the electron-density map in the incorrect space group made no sense in terms of its (lack of) connectivity and in its relationship to the known concanavalin A monomer (and dimer) structure. This forced the re-evaluation of the project.

We have found then that in this crystal the quaternary structure of the protein is the dimer of dimers common to all known concanavalin A structures. However, the packing of these tetramers in the crystal lattice is quite different from that in the saccharide-free or αMM-bound crystal forms. Now that the packing of this crystal structure is known it allows a detailed structural study of concanavalin A complexed with αMG at higher resolution and its comparison with αMM-bound concanavalin A.

We are grateful to SERC for research studentships awarded to TCMW and SJH and to the SERC Molecular Recognition Initiative for a PDRA post for SJH. The data collection was carried out in the Physics Department at the University of York, and the computational analysis reported in the paper was subsequently carried out in the Chemistry Department at the University of Manchester, to both of whom we are very grateful for general support.

The molecular-replacement calculations presented in *Appendix A* were performed at Purdue University during a sabbatical leave of AJK(G) who thanks M. G. Rossmann for his help and support.

4. APPENDIX *A*
Molecular-replacement solution of the cubic complex of concanavalin A with αMG

The structure of this complex should be an ideal case for solution by molecular replacement. Saccharide-free concanavalin A [PDB entries 2CNA (Reeke, Becker & Edelman, 1975) and 3CNA (Hardman & Ainsworth, 1972)] is an excellent model structure because it is an all-β-structure protein and is unlikely to be subject to serious distortion by saccharide binding or by crystallization conditions. Attempts to solve the structure by means of Crowther's fast rotation function failed however, possibly because of the large number of crystallographic symmetry elements in the corresponding Patterson function ($Im\bar{3}$ for $I23$ or $I2_13$ with additional pseudo-symmetry corresponding to $Im\bar{3}m$ as discussed below). The general rotation function (Tong & Rossmann, 1990) proved to be a better choice in this case, although the solution was far from straightforward, as described below.

4.1. *Self-rotation analysis*

The general rotation function (Tong & Rossmann, 1990) allows one to reduce the search for local symmetry to a two-dimensional problem in polar coordinates if the expected local symmetry element can be specified. In the present case, since the asymmetric unit contains a dimer of concanavalin A, a molecular twofold axis is present. Accordingly, the angle κ was fixed at 180°. A two-dimensional search in the polar angles φ and ψ produced one significant peak in the asymmetric unit at $\psi = 90°$. and $\varphi = 45°$. The diffraction data for this search were from the highly precise and complete (98%) 5.4 Å data set for Co,Ca-concanavalin A referred to in this paper (Table 1). However, this proved to be an unfortunate choice because it is only at higher resolution that two additional peaks emerge in the rotation function. This is shown in Table 6 where the self-rotation function peak values from a high-resolution data set (2 Å film data collected at Daresbury) are shown for progressively higher resolution and compared to those from the 5.4 Å data set. The origin of the pseudo-twofold axis at 45°, corresponding to the direction of the face diagonal of the unit cell, is not clear. However, its existence generates additional elements of pseudo-symmetry in the Patterson function corresponding, unfortunately, to space group $Im\bar{3}m$. The two peaks at 34° and 56° (Table 7) are related by this extra symmetry but, as shown in Table 8, only one of these peaks corresponds to the correct orientation of the molecular dyad.

Table 7. *Self-rotation peak values for $\psi = 90°$, $\kappa = 180°$ as a function of resolution*

Resolution range (Å)	Peak heights (as percentage of origin peak) $\varphi = 45°$	$\varphi = 34, 56°$
10–5.5*	28.3	4.2
10–5.5	21.6	11.4
10–4.0	22.9	15.0
10–3.0	27.4	20.2
10–2.5	29.5	23.0

* This is the data set referred to in Table 1 as [Co:Ca]. The remaining entries are based on a 2 Å film data set collected on station 9.6 (Helliwell *et al.*, 1986) at Daresbury (M. Z. Papiz) and processed at York/Manchester (J. Habash). These data will be described in a paper including the 2 Å refined structure of the glucoside (Gleichman *et al.*, to be published).

Table 8. *Cross-rotation peak values for three possible orientations of the molecular twofold axis*

ψ (°)	φ (°)	κ (°)	Rotation function Peak	Rotation function Second	σ Peak	σ Second
90	45	26	3600	1260	2.66	1.43
90	34	90	2100	1970	2.26	2.18
90	56	88	6000	1800	4.15	1.77

4.2. *Cross-rotation analysis*

The dimer model structure for cross rotation was based on the least-squares refined version of the monomer of saccharide-free concanavalin A [space group $I222$, PDB entry 2CNA (Reeke *et al.*, 1975)] produced by 180° rotation of the monomeric asymmetric unit about the crystallographic z axis (*cf.* Derewenda *et al.*, 1989). Structure factors were calculated in a rectangular $P2$ cell of dimensions $a = b = c = 130$ Å. The general rotation function as implemented in *REPLACE* (Tong, 1993) can reduce the cross-rotation search to a one parameter search in the polar angle κ by first aligning the molecular twofold of the model with that of the unknown structure previously deduced from the self-rotation analysis. The three self-rotation peaks at $\psi = 90°$ and $\varphi = 34$, 45 or 56° were tested by this method against the 5.4 Å data set. The peak at $\varphi = 56°$ is clearly the correct solution (Table 7). The angular coordinates of the peak were optimized on a fine grid in the three Eulerian angles. These were used to calculate atomic coordinates for the translation-search model.

4.3. *The translation function*

A structure-factor correlation-function translation search was performed with the program *TF* (Tong, 1993) against the 5.4 Å data set on a 1.68 Å grid for space groups $I23$ and $I2_13$. One significant and well discriminated peak was found for space group $I2_13$ [correlation coefficient = 0.35 (9.6σ), next highest peak = 0.21 (5.1σ)]. No comparable solution was found for space group $I23$ [highest peak = 0.21 (5.0σ), next

peak = 0.20] indicating that the correct space group is $I2_13$.

In a different approach, the same diffraction data were used in the Patterson correlation translation-function calculation with the program *TF* (Tong, 1993). The results were essentially the same as the above but the Patterson correlation calculations were much faster than the structure-factor correlation calculations. In this method it was also possible to partition the search into two two-dimensional searches by suitable selection of symmetry-related asymmetric units.

4.4. *Rigid-body refinement*

The translation-function peak position was refined by a fine-grid search (0.84 Å) in the vicinity of the peak. The result, for which the correlation coefficient improved to a value of 0.42, was used to calculate the coordinates of one asymmetric unit in the $I2_13$ unit cell. This was further refined as two rigid bodies against all observed structure factors for which $F > 2\sigma F$ between 8.0 and 5.4 Å (*X-PLOR*). The final R factor was 0.378.

4.5. *Comparison with the MIR result*

For the purpose of comparison, the calculations described above were repeated using a dimeric model based on the recently published, highly refined 2.0 Å structure of saccharide-free Cd,Ca concanavalin A (PDB entry 1CON; Naismith *et al.*, 1993) that was fitted to the MIR map as described in this paper. The final R factor in this case was 0.343. C_α positions of the MR and MIR solutions have an r.m.s. difference of 0.4 Å confirming that the MR solution is consistent with the MIR solution.

5. APPENDIX *B*
Analyses performed in the incorrect space group (*I*23)

Early work in the X-ray study of the cubic crystal form involved a K_2PtCl_4 isomorphous difference Patterson map, whose interpretation was convincing in space group *I*23. Moreover, the sites obtained had enough chemical proof to proceed further with refinement of the heavy atoms, phasing and then solvent flattening. In this *Appendix* details are given of the *I*23 analysis starting with the isomorphous difference Patterson of the Pt derivative. The $W = 0$ Harker section from K_2PtCl_4 against [Co:Ca] is shown in Fig. 6. The positions of the Pt sites derived from an interpretation in *I*23 are given in Table 9. The proposed solution involved a two-site Pt substitution in an *I*23 unit cell. This indicated a dimer (50 kDa) in the asymmetric unit which is consistent with the results from the crystal density measurements (Yariv *et al.*, 1987). The Harker vectors generated from these proposed sites are marked • on this $W = 0$ Harker section. (Fig. 6).

Table 9. *Fractional positions of the S1 and Pt sites in the I23 cell for the false solution*

Site	*X*	*Y*	*Z*
*S*1	0.1739	0.0463	0.2585
Pt1	0.2403	0.1488	0.1180
Pt2	0.2210	0.1574	0.1610

The Pt sites form a pair 8 Å apart, which is consistent with the known behaviour of K_2PtCl_4 substitution in other crystal forms of concanavalin A (Hardman & Ainsworth, 1972; Reeke *et al.*, 1971; Shoham *et al.*, 1979) where the major site of binding is to the Sδ Met129 residues in the dimer which are part of the hydrogen-bonding interface between the two subunits making a dimer of concanavalin A. This correlation was a significant factor in the acceptance of an *I*23 interpretation of this Pt isomorphous Patterson. Heavy-atom refinement of these two Pt sites was undertaken using the *CCP*4 (Collaborative Computational Project, Number 4, 1994) program *REFINE* using the centric *FHLE* option. SIRAS phasing calculations were made with the *CCP*4 program *PHASE*. A difference Fourier map yielded a possible Cd site involving coefficients Cd:Ca–Co:Ca (two were expected with a dimer in the asymmetric unit). This site was also refined (Table 9) and then an MIR phase calculation performed based on the two-site Pt model and the one Cd site. The mean figure of merit was 0.4.

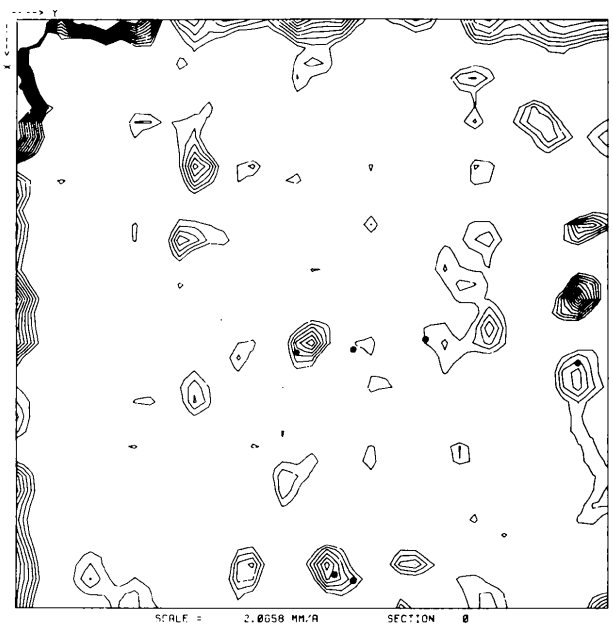

Fig. 6. $W = 0$ Harker section for the K_2PtCl_4 *versus* [Co:Ca] isomorphous difference Patterson map calculated at 5.4 Å. The Harker vectors generated by a two-site Pt *I*23 solution are marked. Map contoured from 10 in intervals of 5. Origin peak value set to 900. Half the unit cell is shown.

A 5.4 Å MIR map of the concanavalin A and αMG complex was then calculated. Representative sections of this map are shown in Fig. 7. This map is noisy but it did not seem random, in that regions of high density were localized into clumps, with contrast against weaker regions of density (*viz* solvent).

Solvent-flattening calculations were than carried out using Leslie's *FFT* version (Leslie, 1987, 1989) of Wang's solvent-flattening package (Wang, 1985) as available in the *CCP*4 program suite. The starting map was subjected to 24 cycles of iterative solvent flattening. The solvent mask was gradually increased from an artificially low value of 40% to a final level of 65% in steps of 5%. The solvent mask was only

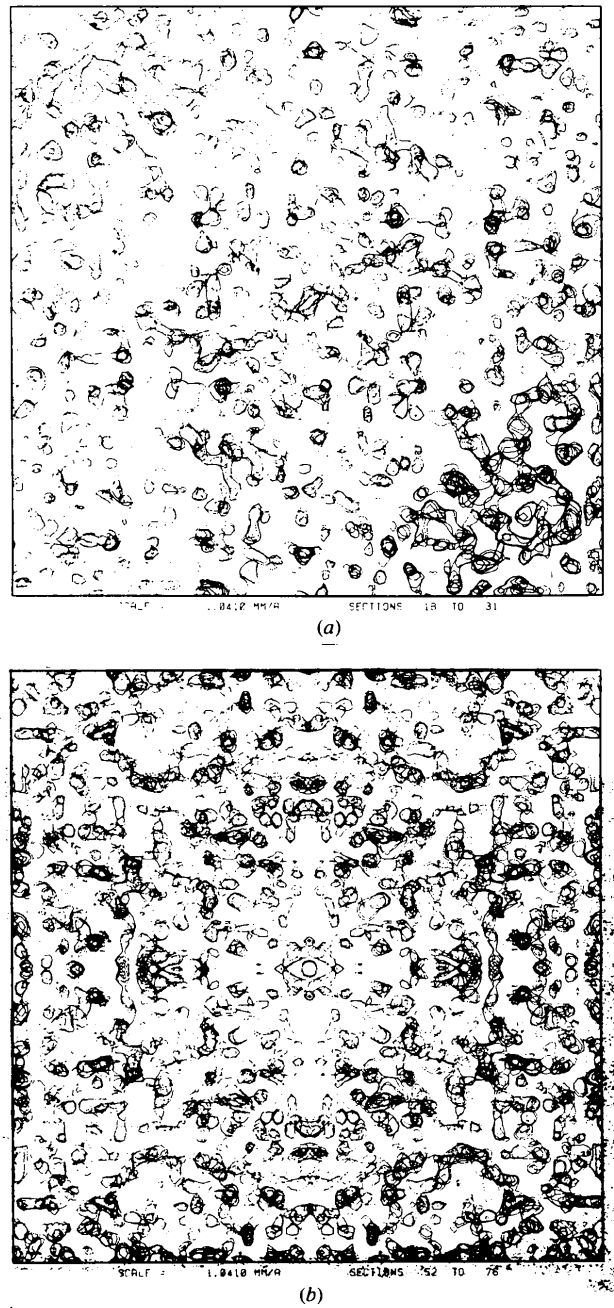

(*a*)

(*b*)

Fig. 7. MIR map at 5.4 Å in *I*23. (*a*) *z* sections 18/128 to 31/128. (*b*) A slab through the (1/2, 1/2, 1/2) position. (*i.e.* Z sections 52/128 to 76/128). The map shows the whole unit cell along *y* and *x* and is contoured from 1.5 r.m.s. in intervals of 1 r.m.s.

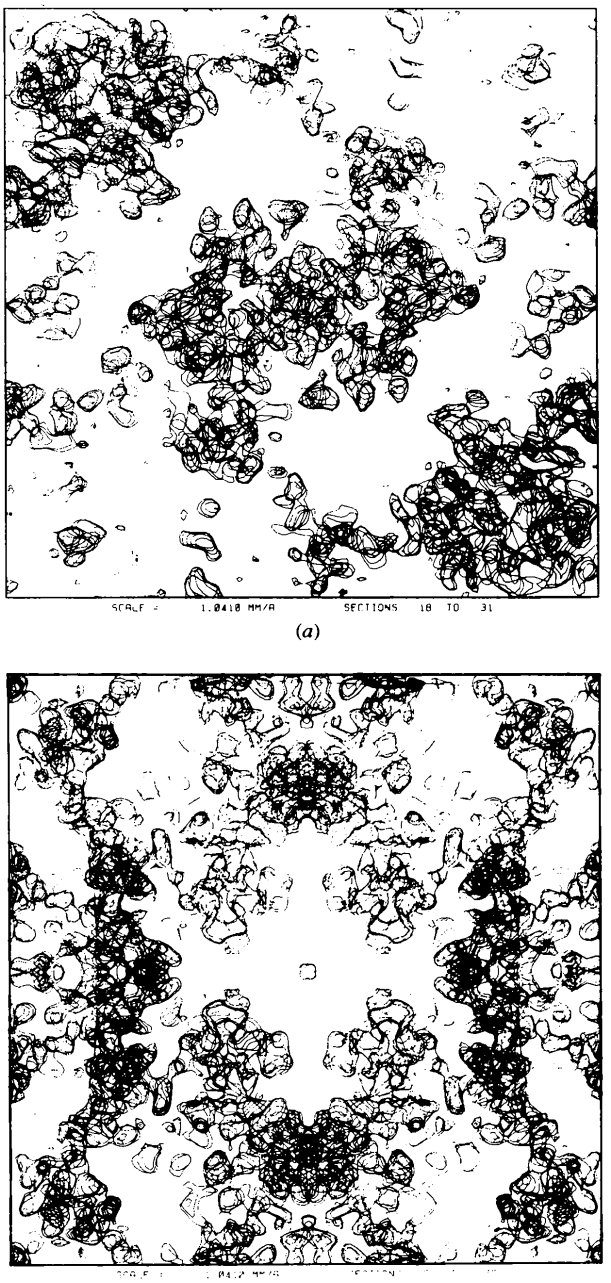

(*a*)

(*b*)

Fig. 8. Same sections as Fig. 7 but after solvent flattening. Contoured from 1 r.m.s. in intervals of 1 r.m.s.

updated when the proportion of solvent was increased. The negative density inside the region defined as protein was not truncated. All data between ∞ and 5.4 Å were included in the calculations. The unit cell was sampled on a 128 × 128 × 128 grid. As the MIR phases were considered poor they were rejected after the first cycle (Vellieux *et al.*, 1989), rather than phase combined with the phases generated from the back-transformed maps. Sim weights for the Fourier components of the new maps were calculated using the *CCP*4 program *COMBINE*. No calculated *F*'s were used in any of the maps, except in the envelope-generation stage (Leslie, 1989). No amplitude combination was performed so that observed *F*'s were used throughout. The course of the calculations was monitored by examining the phase-improved maps and following the *R* factor, map correlation and mean phase change between each cycle.

Fig. 8 shows the same sections as in Fig. 7 but after 24 cycles of solvent flattening. Fig. 9 shows the crystallographic *R* factor and correlation coefficient between

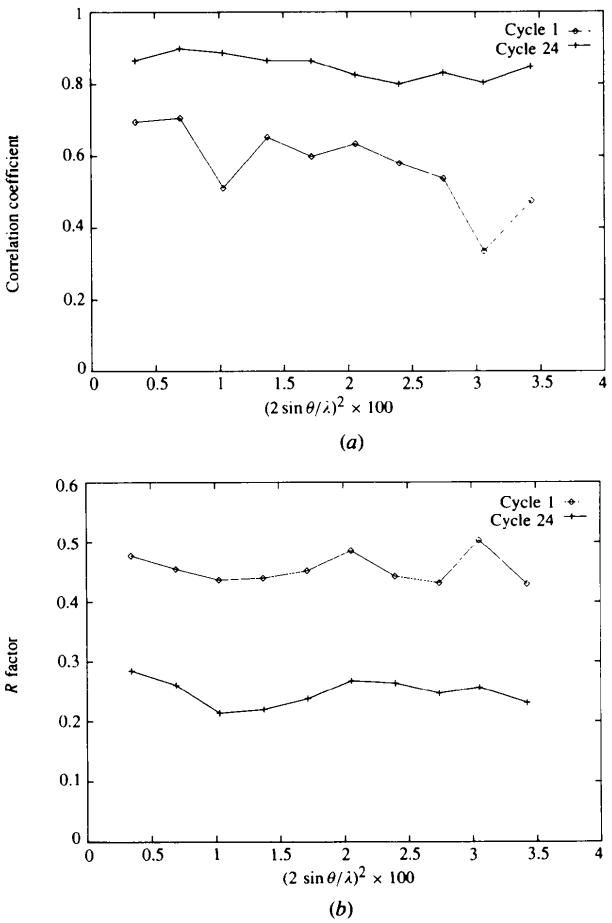

Fig. 9. (*a*) Correlation coefficient and (*b*) *R* factor between F_{obs} and F_{calc} for the *I*23 maps at cycle 1 and cycle 24 of the solvent-flattening procedure.

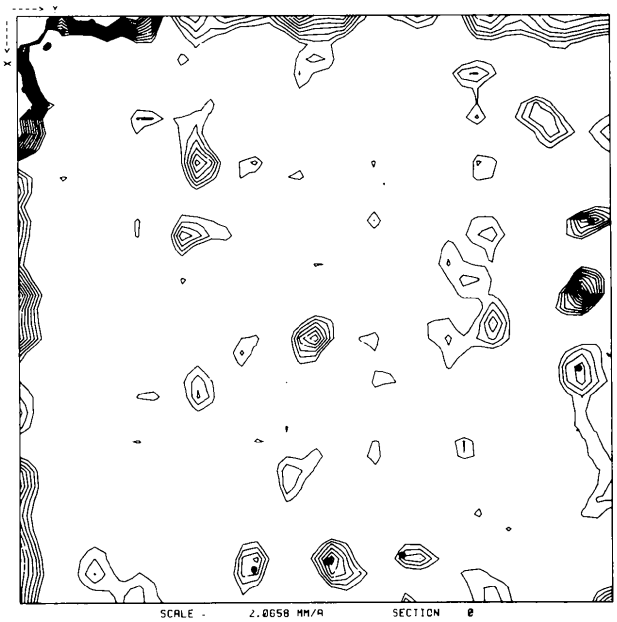

Fig. 10. The correct $I2_13$ interpretation of the K_2PtCl_4 Patterson. The vectors from the two major Pt positions were located from difference Fourier maps. These are marked • on the $W = 0$ Harker section. Half the unit cell is shown.

observed *F*'s and those calculated from the flattened map at the beginning (cycle 1) and end (cycle 24) of the calculations. The *R* factor is defined as,

$$R = (\sum |F_{obs} - F_{calc}|)/\sum |F_{obs}|,$$

and the correlation coefficient,

$$C = \left[\sum_h (F_{obs} - \langle F_{obs}\rangle)(F_{calc} - \langle F_{calc}\rangle)\right] \times \left[\sum_h (F_{obs} - \langle F_{obs}\rangle)^2 \sum_h (F_{calc} - \langle F_{calc}\rangle)^2\right]^{-1/2}.$$

However, even though this map showed 'solvent contrast' it simply could not be interpreted. A completely new approach led to the correct structure in $I2_13$ and with the K_2PtCl_4 finally reinterpreted according to space group $I2_13$ as in Fig. 10.

References

Blow, D. M. & Crick, F. H. C. (1959). *Acta Cryst.* **12**, 794–802.
Collaborative Computational Project, Number 4 (1994). *Acta Cryst.* **D50**, 760–763.
Derewenda, Z. (1989). *Acta Cryst.* A**45**, 227–234.
Derewenda, Z. & Helliwell, J. R. (1989). *J. Appl. Cryst.* **22**, 123–137.
Derewenda, Z., Yariv, J., Helliwell, J. R., Kalb (Gilboa), A. J., Dodson, E. J., Papiz, M. Z., Wan, T. C. M. & Campbell, J. W. (1989). *EMBO J.* **8**, 2189–2193.
Dodson, E. J. & Vijayan, M. (1971). *Acta Cryst.* B**27**, 2402–2411.

Greer, J., Kaufman, H. W. & Kalb, A. J. (1970). *J. Mol. Biol.* **48**, 365–366.
Hardman, K. & Ainsworth, J. (1972). *Biochemistry*, **11**, 4910–4919.
Harrop, S. J., Naismith, J. H., Emmerich, C., Habash, J., Weisgerber, S., Kalb (Gilboa), A. J., Yariv, J. & Helliwell, J. R. (1993). *Acta Cryst.* A**49**. Suppl. *C*94.
Helliwell, J. R., Papiz, M. Z., Glover, I. D., Habash, J., Thompson, A. W., Moore, P. R., Harris, N., Croft, D. & Pantos, E. (1986). *Nucl. Instrum. Methods A*, **246**, 617–623.
Howard, A. J., Gilliland, G. L., Finzel, B. C., Poulos, T. L., Ohlendorf, D. H. & Salemme, R. (1987). *J. Appl. Cryst.* **20**, 383–387.
Jones, T. A. (1978). *J. Appl. Cryst.* **20**, 24–31.
Kabsch, W. (1976). *Acta Cryst.* A**32**, 922–923.
Kalb (Gilboa), A. J., Yariv, J., Helliwell, J. R. & Papiz, M. Z. (1988). *J. Cryst. Growth*, **88**, 537–540.
Leslie, A. (1987). *Acta Cryst.* A**43**, 134–136.
Leslie, A. (1989). *Proceedings of the Daresbury Study Weekend DL/SCI/R26*, pp. 13–24. Warrington: Daresbury Laboratory.
Naismith, J. H., Emmerich, C., Habash, J., Harrop, S. J., Helliwell, J. R., Hunter, W. N., Raftery, J., Kalb (Gilboa), A. J. & Yariv, J. (1994). *Acta Cryst.* D**50**, 847–858.
Naismith, J. H., Habash, J., Harrop, S. J., Helliwell, J. R., Hunter, W. N., Wan, T. C. M., Weisgerber, S., Kalb (Gilboa), A. J. & Yariv, J. (1993). *Acta Cryst.* D**49**, 561–571.
Reeke, G. N. Jr, Becker, J. W. & Edelman, G. M. (1975). *J. Biol. Chem.* **250**, 1525–1547.
Reeke, G. N. Jr, Becker, J. W. & Quiocho, F. A. (1971). *Cold Spring Harbor Symp. Quant. Biol.* **36**, 272–284.
Shoham, M., Kalb, A. J. & Pecht, I. (1973). *Biochemistry*, **12**, 1914–1916.
Shoham, M., Yonath, A., Sussman, J. L., Moult, J., Traub, W. & Kalb (Gilboa), A. J. (1979). *J. Mol. Biol.* **131**, 137–151.
Tong, L. (1993). *J. Appl. Cryst.* **26**, 748–751.
Tong, L. & Rossmann, M. G. (1990). *Acta Cryst.* A**46**, 783–792.
Tronrud, D., Ten Eyck, L. & Matthews, B. W. (1987). *Acta Cryst.* A**43**, 489–501.
Vellieux, F. M. D., Groendijk, H., Huitema, F., Swarte, M. B. A., Drenth, J. & Hol, W. G. J. (1989). *Proceedings of the Daresbury Study Weekend DL/SCI/R26*, pp. 88–99. Warrington: Daresbury Laboratory.
Wang, B. C. (1985). In *Methods in Enzymology*, Vol. 115, edited by H. Wyckoff, C. H. W. Hirs & S. N. Timasheff. New York: Academic Press.
Weinzierl, J. & Kalb, A. J. (1971). *FEBS Lett.* **18**, 268–270.
Yariv, J., Kalb (Gilboa), A. J., Helliwell, J. R., Papiz, M. Z., Bauminger, E. R. & Nowik, I. (1988). *J. Biol. Chem.* **263**, 13508–13510.
Yariv, J., Kalb (Gilboa), A. J., Papiz, M. Z., Helliwell, J. R., Andrews, S. J. & Habash, J. (1987). *J. Mol. Biol.* **195**, 759–760.